Journal of Applied Polymer Science

WILEY

Applied Polymer SCIENCE

RESEARCH ARTICLE OPEN ACCESS

Chitosan-Silanized Hexagonal Boron Nitride Nanocomposite Films and Properties

Zuhal Yılmaz[1] | Yapıncak Göncü[2] | Nuran Ay[3]

[1]Bilecik Şeyh Edebali University, Söğüt Vocational School, Bilecik, Turkey | [2]Osmangazi University, Engineering Architecture Faculty, Department of Biomedical Engineering, Turkey | [3]Eskişehir Technical University, Engineering Faculty, Department of Materials Science and Engineering, Turkey

Correspondence: Zuhal Yılmaz (zuhal.guven@bilecik.edu.tr)

Received: 7 November 2024 | **Revised:** 27 January 2025 | **Accepted:** 27 March 2025

Funding: This work was supported by the Scientific Research Project Commission of Eskişehir Technical University (grant number: 22GAP257).

Keywords: biodegradable | crosslinking | manufacturing | packaging | structure-property relationships

ABSTRACT

In this study, chitosan-silanized hexagonal boron nitride (hBN) nanocomposite films were developed using the solution casting method. Unlike chitosan-hBN studies, silanization of hBN with Vinyl trimethoxy silane (VTS) formed hydrogen bonds. In the swelling ratio, an improvement of 18.6% was observed with the addition of hBN compared to pure chitosan. A water vapor permeability of $2.54 \times 10^{-10}\,g^{-1}\,s^{-1}\,Pa^{-1}$ was observed for pure chitosan; however, this value decreased to $1.47 \times 10^{-10}\,g^{-1}\,s^{-1}\,Pa^{-1}$ with the addition of 0.9% hBN. A rate of oxygen permeability of 542.2 cm^3/m^2 day was observed for composites incorporating hBN, significantly lower than the 1350.79 cm^3/m^2 day rate recorded for chitosan. Increasing the hBN addition enhanced the composite films' thermal stability and improved the UV barrier properties. Adding hBN did not negatively affect the NaOH resistance of composite films. The sample containing 0.6% hBN exhibited the highest contact angle values of 97.59 ± 2.68. The research recorded a tensile strength of 77.9 MPa and Young's modulus of 6299.86 MPa for the sample containing 0.9% hBN. The composites showed cell viability in the cytotoxicity tests conducted at three different time periods and at all concentrations. It has been determined to have good biocompatibility and does not show toxic effects.

1 | Introduction

Synthetic plastics, such as polystyrene, polypropylene, polyethylene, poly methyl methacrylate, and polyvinyl chloride, are widely used in various aspects of our everyday routines owing to their favorable characteristics of lightweight, inertness, and cost-effectiveness [1–5]. Plastics, which accumulate in the natural environment because they are resistant to microbial degradation, are undesirable pollutants for soil, seas, and rivers. Many synthetic polymers are produced and used that are resistant to chemical and physical degradation. With the increasing use of plastics, the inadequacy of traditional methods such as landfilling, recycling, and incineration for the disposal of their wastes has become apparent. However, biodegradable plastics are coming out as one option for solving environmental problems [6, 7]. Biodegradable plastics offer significant advantages because composting them with organic waste enriches the soil. The process of decomposing biodegradable plastics will aid in the reduction of landfills by minimizing the amount of waste. Moreover, the utilization of microbial and enzymatic treatment allows for the recycling of plastic waste into valuable monomers and oligomers, leading to a decrease in labor costs for its removal from the environment [8].

Chitin, poly (β-(1 → 4)-N-acetyl-D-glucosamine), is a natural polysaccharide of great importance, first described in 1884. This biopolymer is synthesized by many living organisms and is the second most abundant polymer after cellulose in terms of the amount of chitin produced annually in the world [9]. Every year, crustaceans, mollusks, insects, fungi, and related

organisms produce about 100 billion tonnes of chitin on Earth [10]. Although chitin has functional properties such as biocompatibility, bioactivity, biodegradability, and high mechanical strength, it has limited use due to its poor solubility [11, 12]. This interest leads to chitosan, the main derivative of chitin. Chitin is converted to chitosan by enzymatic or chemical processes [10, 12]. Chitosan is a random copolymer derived from the alkaline deacetylation of chitin, which consists of D-glucosamine and N-acetyl-D-glucosamine units connected by β-1,4 glycosidic linkages. The ratio between the two units is considered the degree of deacetylation [11, 13]. The solubility of chitosan in aqueous acidic environments is observed when its degree of deacetylation approaches 50% [7]. Dissolving chitosan in acidic media leads to the protonation of its amino groups, causing the polymer to become cationic, which allows it to interact with various types of molecules [12].

Active food packaging involves packaging food with materials that provide enhanced functionality, such as antimicrobial and antioxidant properties, through incorporating active compounds [14]. Presently, active packaging stands as one of the most dynamic technologies employed to ensure the preservation of food quality, safety, and perceptual attributes. The active packaging positively interacts with the product and the environment to improve/maintain food quality longer than conventional packaging [15]. Chitosan has emerged as a highly promising biodegradable packaging material among various biopolymers [16]. However, the mechanical properties are insufficient to meet the diverse range of applications. The food packaging industry faces limitations in its use of biopolymers because of issues such as poor barrier and mechanical properties, challenges in scaling up production, and lack of stability in an aqueous environment [9]. The physical properties of chitosan can be enhanced by loading with nanofillers [17–21].

Hexagonal boron nitride (hBN) has a layered structure very similar to graphite and has many unique engineering properties and uses. In recent years, its properties and biocompatibility as an antibacterial material have been investigated, and its use in different fields has been developed by utilizing this effect [22–25]. Studies on the use of boron nitride in polymer composite production are increasing [26–28]. The utilization of hBN as processing aids in production proves successful, owing to the lubricating properties derived from its graphite-like layered structure. This not only eliminates melt fracture but also postpones cleavage failures to significantly higher slip rates. hBN can provide smooth surface shaping as a stress reliever in the polymer [29–33].

The properties of polymers, composites, and scaffolds can be enhanced through incorporating hBN and boron nitride nanotubes (BNNT), owing to their low toxicity, antibacterial effects [24, 25], high mechanical strength, and chemical stability [34–36]. Recent studies have explored chitosan-hexagonal boron nitride (hBN) nanocomposite films for various applications. These films exhibit enhanced UV shielding, with up to 98.51% UV-A and 96.40% UV-B resistance, and improved gas barrier properties, reducing oxygen and carbon dioxide permeability by over 94% [37]. The addition of hBN nanoparticles to chitosan films also improves water vapor barrier ability, thermal stability, and mechanical properties [37, 38]. Chitosan-hBN nanocomposites show increased dielectric constants, reaching ~1200 at 5 wt% hBN loading [39]. Furthermore, nanocomposites containing polyhydroxyalkanoate, chitosan, and hexagonal boron nitride (PHA/Ch-hBN) have been reported to exhibit effective antimicrobial and biocompatibility properties that may be suitable for antibacterial and biomedical applications [24]. Incorporating hBN into the chitosan polymer film not only improves its mechanical properties during the production process but also the physical properties of the final product, including oxygen permeability and water absorption [38, 40]. In the films produced using chitosan containing borax (B) and boron nitride (BN) as food packaging, antioxidant and antimicrobial films with high thermal stability and low water vapor loss were obtained [41]. These enhanced properties make chitosan/hBN nanocomposite films promising candidates for food packaging and biomedical applications.

In the studies described above, boron nitride was used by dispersing it without any pretreatment. However, the modification of the hBN surface significantly impacts polymers, facilitating exfoliation and promoting proper dispersion of the nano-sized material within the composite [42]. In this respect, it was hypothesized that the properties of chitosan-hBN films could be improved by functionalizing hBN to change the surface chemistry and improve interface interactions. Silane coupling agents, which are extensively employed as surfactants to modify or functionalize the surfaces of inorganic particles, show promise [43]. Vinyl trimethoxy silane (VTS) is a silicone-containing crosslinker, and the crosslinking prevents the chains from breaking down under stress conditions [44]. There are successful studies using VTS in the surface functionalization of hBN [26, 42, 43].

In this study, chitosan-silanized hBN composite films were produced by the solution casting method and various physicochemical properties of the films were investigated to understand the effect of silanized hBN addition on the film structure. Unlike other studies in the literature, this study aimed to enhance chitosan's characteristics by developing surface-modified hBN nano-filled composites to address the limitations of chitosan in its application within the food packaging industry. The synthesis of chitosan-hBN nanocomposite, which is biodegradable in the food packaging industry and has high mechanical, physical, and chemical properties, extends the shelf life due to its low oxygen permeability and nontoxic, has been successfully achieved.

2 | Experimental Procedure

2.1 | Materials

Chitosan (Glentham) (medium molecular weight, Mw: 1,250,000, degree of deacetylation ≥ 90%), hBN (Bortek Boron Technologies and Mechatronic Inc., Turkey) with a D50 grain size of 120 nm, and Vinyl trimethoxy silane (VTS) (MERCK) were used in the study. For sample preparation, 1% diluted acetic acid (Acros Organics, 99.7% purity) was used as a solvent, sodium sulfate (AFG Bioscience, 99% purity) for crosslinking, and sodium hydroxide (NaOH) (Sigma Aldrich, 99%–100.5% purity) for chemical resistance testing. L929 cells (L929 Cell

originated from ATCC CCL-1) were used for cytotoxicity tests. The cells were cultured in 10% Fetal bovine serum (FBS) (Pan Biotech P30-1301), Eagle's minimum essential medium (EMEM) (ATCC) and with the addition of Trypsin–EDTA (Gibco 15400054).

2.2 | Silanization of Boron Nitride Particles

The functionalization of the surface of boron nitride particles was carried out according to Seyhan et al. [43]. The flow chart of the silanization process is given in Figure 1. Vinyl trimethoxy silane (VTS) was used for functionalization. Briefly, 3 g of BN powder was stirred in nitric acid solution at 70°C and allowed to rest for 1 night. The BN particles were dehydrated by vacuum filtration, dried in an oven at 80°C, then ground in an agate mortar and sieved. A mixture of ethanol and deionized water (4:1) was prepared for silanation. pH was adjusted to 4 using 95% sulfuric acid. The silane coupling agent was added to the mixture at 3 wt% of BN and stirred. After adding the surface hydroxylated BN powder to the solution, it was stirred with a magnetic stirrer for 1 h and dispersed in an ultrasonic bath. The solution was allowed to stand for a night during the aging process and filtered by vacuum filtration. The cake was washed with methanol and distilled water to remove silane residues. It was dried in an oven at 110°C for 5 h to form the siloxane network.

2.3 | Preparation of Chitosan-hBN Nanocomposite Films

The flow chart of the nanocomposites production process is given in Figure 2. The chitosan solution was prepared by dissolving 1 g of chitosan in 99 mL of diluted acetic acid (1% vol/vol) while subjecting the mixture to magnetic stirring at 500 rpm and a temperature of 50°C for 5 h. To disperse three different concentrations of hBN silanized with VTS at 0.3, 0.6, and 0.9 wt%, a magnetic stirrer was employed to mix the substances in 50 mL of distilled water for 48 h. The samples

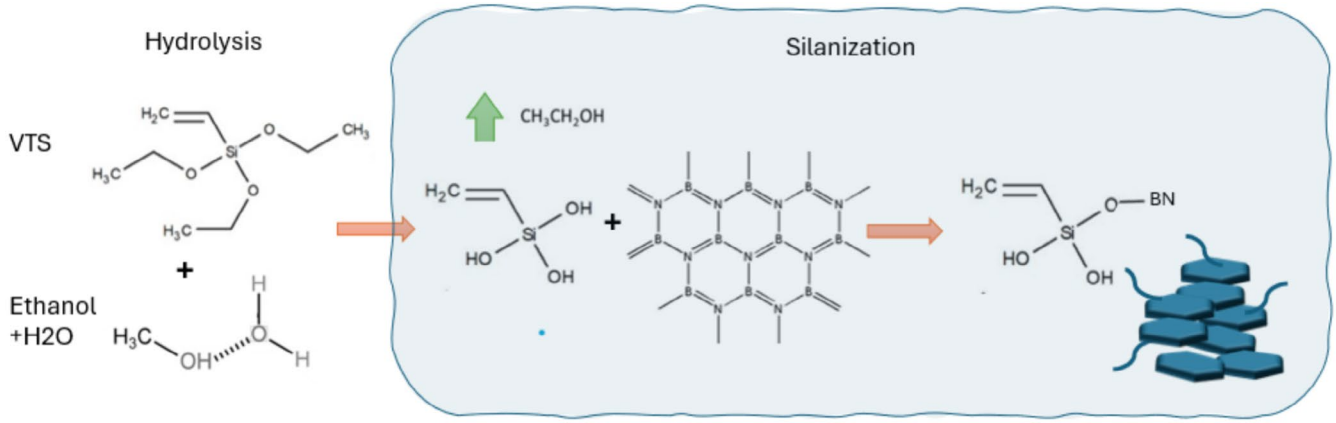

FIGURE 1 | The flow chart of the salinization process. [Color figure can be viewed at wileyonlinelibrary.com]

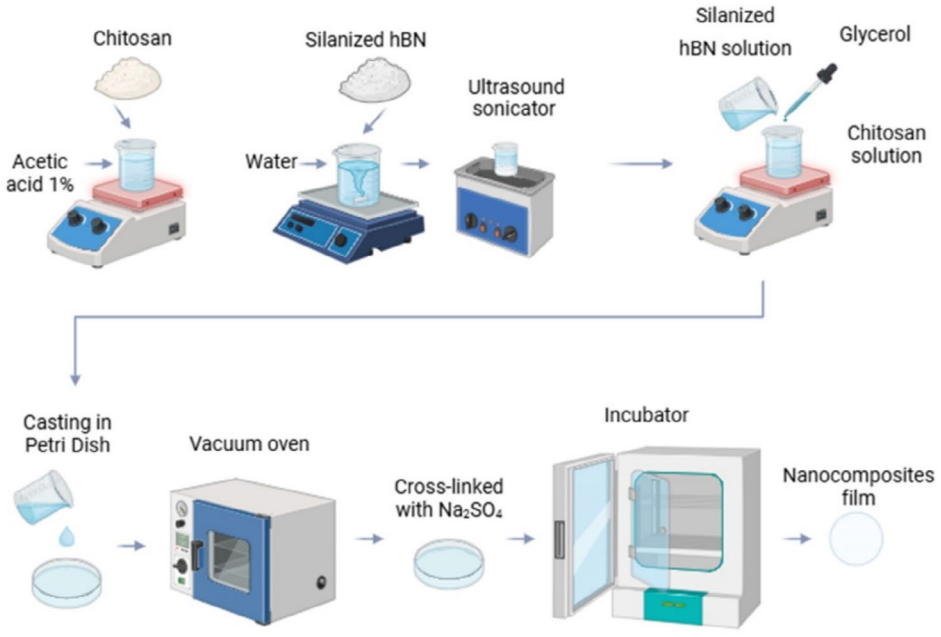

FIGURE 2 | The flow chart of the nanocomposites production process. [Color figure can be viewed at wileyonlinelibrary.com]

containing silanized hBN were coded as S-0.3, S-0.6, and S-0.9. The same procedure prepared pure chitosan film (S-0) for comparison with other samples. Subsequently, the mixture was sonicated into an ultrasonic sonicator for 90 min. The hBN water suspension was introduced into the chitosan solution and stirred for 18 h at room temperature. 1% vol/vol glycerol was added to the mixture was followed by an additional 1 h of stirring. The chitosan-hBN solutions were poured into petri dishes to form thin films. These films were then placed in a vacuum oven (Nucleon) at a temperature of 25°C for a duration of 2 h to allow solvent evaporation and bubble removal. Following this, the films were dried in a conventional oven at 50°C for 24 h to remove the remaining solvent. Chitosan exhibits solubility in diluted solutions of both organic and inorganic acids. Because the chitosan solution is prepared in acetic acid, the acid will remain in the film after evaporation of the water. When in contact with food products, these films can dissolve and degrade. In order to achieve water-insoluble films, chitosan films were cross-linked with Na_2SO_4, a nontoxic substance. The formation of crosslinking was accomplished through an ionic interaction between the positively charged functional groups of chitosan and sulfate anions [45]. Na_2SO_4 aqueous solution (15 wt%) was prepared for the crosslinking process. The removal of the dried films from the petri dishes was followed by immersion in a Na_2SO_4 solution and crosslinking for 1 h. The films were washed with distilled water and dried in an oven at 50°C. Following that, the film samples were conditioned in an incubator (Nüve GC 400) chamber at 25°C and 50% humidity for 48 h.

2.4 | Characterization

Fourier transform infrared (FTIR) spectra of the samples and silanized hBN were measured in the wavelength range 400–4000 cm^{-1} using a BRUKER, TENSOR 27 IR spectrometer. The hBN and film structure were examined using scanning electron microscopy (SEM, ZEISS SUPRA 50VP) at 10 kV and 6 kV voltage, respectively. The crystal structures of the films were determined using an x-ray diffractometer (XRD) (Rigaku, Miniflex 600) with CuK_α radiation ($\lambda = 1.54$ Å) at a scan rate of 2°/min in the range 2θ 5°–50°. Thermogravimetric analysis (TGA) was performed with a Netzsch STA 449F3 instrument by measuring up to 500°C at a heating rate of 10°C/min in a nitrogen environment. Contact angle measurements were conducted using a drop shape analyzer ATTENTION in order to determine the hydrophobicity of the thin film. The film samples adhered to a glass plate with adhesive tape. Following this, a constant volume of drops of pure water was applied to the surface of the samples using a 3 μL injector to measure the contact angle. Subsequently, the contact angle of both sides of the water droplet was measured. All measurements were performed at room temperature in three repetitions. To determine the opacity of the films, transmittance values were measured in the wavelength range from 200 to 850 using a UV spectrophotometer (SHIMADZU MPC-603). The opacity was calculated according to Equation (1) following [46, 47]:

$$\text{Opacity} = \text{Abs}_{600} / \text{d} \tag{1}$$

where Abs_{600} and d are the values of absorbance at 600 nm and film thickness (mm), respectively.

The blocking effect of hBN to UV transmission for the chitosan film was calculated with Equation (2) as follows [48]:

$$\text{Blocking effect} = \frac{T_{chitosan} - T_{composite}}{\textit{the percent of hBN with respect to chitosan}} \tag{2}$$

where $T_{chitosan}$ and $T_{composite}$ refer to the percent transmittance for the chitosan and the composite film, respectively. All measurements were performed in three repetitions.

The color of the films was assessed using a colorimeter (Konica Minolta) without plating. L*, a*, and b* values were measured. All measurements were repeated 3 times and averaged L (white = 100, black = 0), a (green = −60, red = +60) and b (blue = −60, yellow = +60) are the measured values.

2.5 | Water Absorption Tests

Water absorption of film samples was evaluated using swelling values [38, 49]. The film samples were divided into 2 cm × 2 cm pieces and subsequently measured for weight. The placement of every sample into a petri dish, each containing a precise volume of 20 mL of distilled water and kept at 25°C for 24 h, was reached. Swollen samples were removed from the distilled water, dried with filter paper to eliminate any remaining droplets, and subsequently reevaluated in terms of weight. The swelling ratio was calculated according to Equation (3) following:

$$\text{Swelling ratio}\,\% = \left[\left(W_s - W_d\right) / W_d\right] \times 100 \tag{3}$$

where Ws and Wd are the weights of the swollen and dry samples, respectively. All measurements were performed in three repetitions.

2.6 | Equilibrium Moisture Content (MC)

To calculate the equilibrium moisture content (MC) of the films, the film samples were cut into 2 cm × 2 cm pieces and subsequently measured for weight. The samples were dried at 100°C to reach equilibrium, and then the weight loss was measured. The MC was calculated using Equation (4) following [38, 49]:

$$\text{MC}\,\% = \left[\left(W_w - d_d\right) / W_w\right] \times 100 \tag{4}$$

where W_d is the weight after drying, and W_w is the initial weight.

2.7 | Water Vapor Permeability (WVP) Tests

Water vapor permeability (WVP) test was performed according to ASTM-E96. A petri dish (6 cm in diameter) was filled with roughly 20 mL of distilled water, leaving a gap of ~1 cm between

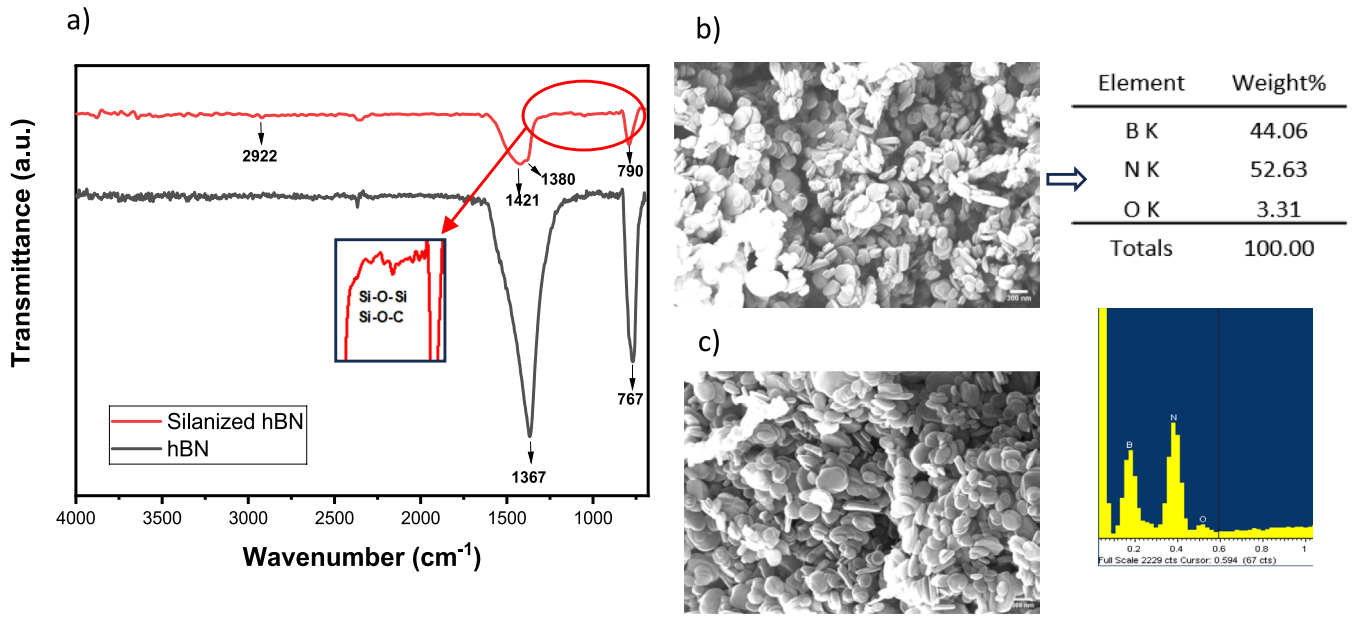

FIGURE 3 | (a) FTIR spectrum of hBN and silanized hBN (b) SEM image and EDS analysis of silanized hBN (c) hBN SEM image. [Color figure can be viewed at wileyonlinelibrary.com]

the water surface and the dish's top. The films were sealed to the top of the dish with water sealing tape. Following the film-sealed petri dishes were weighed. Subsequently, the films were conditioned in an incubator at 25°C and 75% humidity, and weights were measured after 24 h. The WVP was calculated according to Equation (5) following [50]:

$$\mathrm{WVP}\left(\mathrm{g^{-1}s^{-1}Pa^{-1}}\right) = (\mathrm{w}/\mathrm{t}) \cdot \gamma \cdot (\mathrm{A})^{-1} (\Delta \mathrm{p})^{-1} \quad (5)$$

where w is the weight loss of the petri dish (g), t is the time (s), γ is the film thickness (m), A is the cross-sectional area of the film (m^2) and Δp is the vapor pressure difference (3167.2 Pa at 25°C). All measurements were performed in three repetitions.

2.8 | Oxygen Transmission Rate (OTR)

Oxygen permeability (unit: $cm^3\,m^{-2}\,day^{-1}$) was measured using an Okstran instrument (Versoperm Mk VI) at a flow rate of 200 mL, 23°C, and 50% relative humidity, using 10 cm film samples.

2.9 | Chemical Resistance

In order to evaluate the chemical resistance, the samples were kept in 25 mL of dilute 1 M NaOH solution in a closed container for a period of 10 weeks and weighed at weekly intervals. Weight changes were observed. For each sample, three replicate controls were performed according to the procedure described in the paper [17].

2.10 | Mechanical Properties

Tensile tests were performed using Instron 5944 according to ISO 527-2 using a 5 cm long specimen at a head speed of 5 mm min^{-1}, 23°C, and 50% humidity environment [51]. The experiments were performed in four repetitions.

2.11 | Cytotoxicity

To investigate the cytotoxicity of the film, the L929 cell line was used. The L929 cell line was cultured.

EMEM supplemented with 10% FBS (Pan Biotech P30-1301) until reaching a confluence of 70% or higher (Pan Biotech P30-1301) (Doubling Time: 22–26 h). The films were sterilized under the UV lamp. Subsequently, the films were kept in EMEM medium at a concentration of 1 mg mL^{-1} for 1 day in an incubator at 5% CO_2, 37°C, and 95% humidity. At the end of the period, the particle-free supernatant portion of the solution was used in the study. Trypsin–EDTA (Gibco, 15400054) was added to the cells that reached 70% confluence and above in the flask and kept at 37°C in 5% CO_2. When cells were observed to dissociate under an inverted microscope (Zeiss Primovert, Germany), a medium containing 10% FBS was added. Counting was performed on a Logos Luna II device using trypan blue (Gibco, 1525061). The film to be tested for cytotoxicity was added into 96-well plates, and 10% FBS medium was added to it with 10^4 cells per well.

In the Cytotoxicity application Assay, a minimum of three replicate wells was created for each group to enable repeated analysis. Every sample was tested at five different concentrations and three different time points. After the application of the material, the cells were not removed from the incubator for the time to be tested. At the end of the time, the WST-8 solution was added. After 2 h, readings were taken at 450 and 630 nm wavelengths in the cell culture dish. The cell viability% was determined according to Equation (6) following:

$$\text{Cell viability}\,\% = \frac{\text{Test well} - \text{Blank}}{\text{Negative Control} - \text{Blank}} \times 100 \quad (6)$$

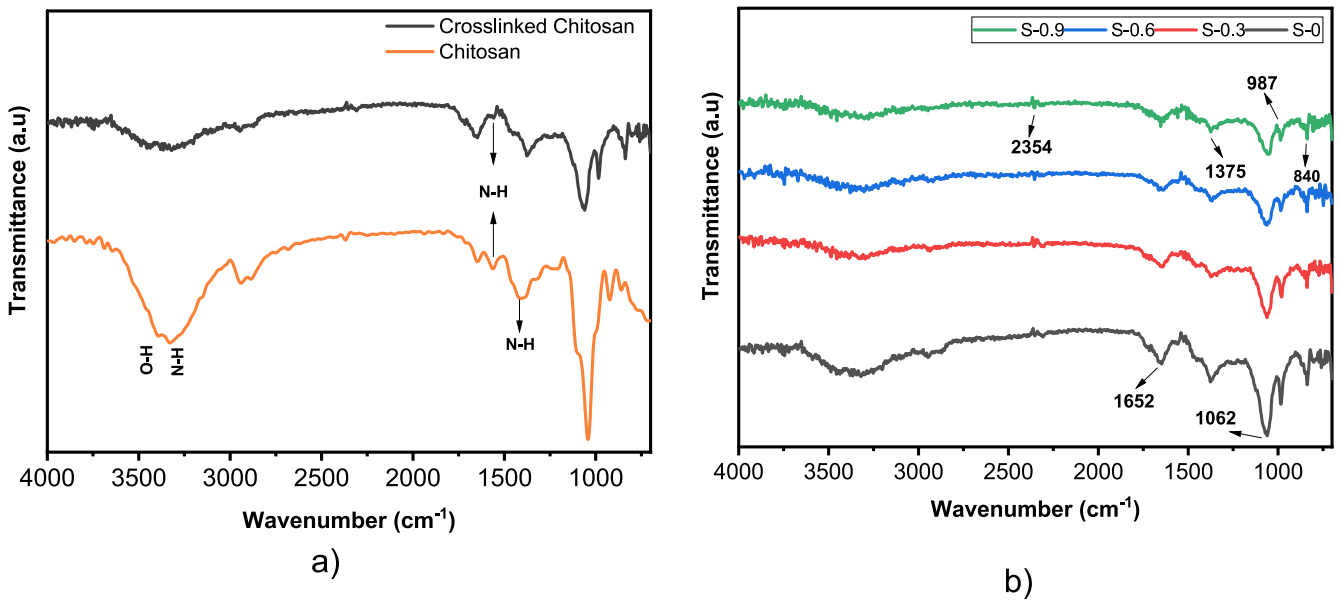

FIGURE 4 | FTIR spectra of (a) chitosan and chitosan cross-linked (b) films with different amount addition of silanized hBN. [Color figure can be viewed at wileyonlinelibrary.com]

3 | Results and Discussion

3.1 | Characterizations

The result of the FTIR analysis of hBN and VTS-silanized hBN powders is shown in Figure 3a. At 1367 and 767 cm^{-1}, the FTIR spectrum exhibits two notable peaks associated with hBN. The peak at 1367 cm^{-1} can be attributed to the B—N stretching vibrations of sp^2-bonded hBN and the peak at 767 cm^{-1} to the B—N—B bending vibrations [52, 53]. After silanization of the hBN with VTS, the new peak at 2922 cm^{-1} was observed to show up, which was associated with symmetric —CH_2 stretching vibrations [43]. Moreover, Si—O—Si and Si—O—C stretchings were associated with weak absorbances between 1225 and 995 cm^{-1}, caused by the condensation of VTS on the surface of hBN [42]. The peak at 1421 cm^{-1} can be attributed to OH groups originating from the B—OH band formed by hydroxylation. Additionally, shifts in the B—N and B—N—B vibration peaks were observed compared to hBN. After silanization, the vibration of B—N stretching shifted from 767 to 790 cm^{-1}, and the vibration of B—N—B shifted from 1367 to 1380 cm^{-1}. The shifts in the hBN peaks coincide with the —CH3 vibration peaks of VTS and may have occurred for this reason [42]. All these results provide evidence that the hBN silanization process was successfully carried out. The SEM images and EDS analysis of silanized hBN (Figure 3b) as well as virgin hBN (Figure 3c) are presented. Hemoglobin-like morphology was observed in all samples with dimensions below 300 nm. No significant morphological differences were observed between the two images. This outcome is consistent with the known limitations of the scanning electron microscope in terms of resolution and imaging capacity. A more definitive conclusion was reached through FTIR analysis. Additionally, the EDX analysis did not detect the presence of any residual chemicals in the silanization process.

FTIR analysis of chitosan and composite films is given in Figure 4. 3550–3200 cm^{-1} is attributed to O—H and N—H stretching of primary amine functional groups. N—H bending of the primary amine functional groups occurs at 1560–1420 cm^{-1} [45, 54]. It was found that the intensity of N—H bending at 1560 and 1420 cm^{-1} decreased after crosslinking [55] (Figure 4a). This is supported by broadening and decrease in the band intensity between 3200 and 3550 cm^{-1}, which comprises N-H stretching and O—H stretching vibrations resulting from the overlapping of the hydroxyl and amino groups [56, 57]. Additionally, the sodium sulfate crosslinking of the chitosan film results in a significant increase in the peak intensity at 1375 cm^{-1} attributed to amid III [58].

FTIR spectra of hBN-added films are given in Figure 4b. The peaks at 2354 and 1062 cm^{-1} can be attributed to C—O stretching of carbonyl groups [38, 46, 59]. The 1652 cm^{-1} peak corresponds to the stretching of the C=O bond in amide I [38, 45, 55]. A band observed at 1375 cm^{-1} [60] showed CH3 symmetric deformations. The peak at 987 cm^{-1} is thought to belong to = C—H out-of-plane bending [61]. The peak positions of chitosan are unchanged in the composite, but there is a decrease in peak intensities with the addition of hBN. N—H and OH stretches at 3550–3200 cm^{-1} were found to decrease due to the increase in the amount of BN. The literature reports that the formation of covalent bonds between silanes and chitosan can only proceed through hydroxyl groups in chitosan because strong Si—O bonds are formed instead of weak Si—N bonds [44, 62]. The decrease in the vibrational intensity of the hydroxyl groups is evidence that the silane binds effectively with chitosan.

Figure 5 shows the XRD pattern of the samples and silanized hBN. Chitosan is a partially crystalline polysaccharide with a regular chain. It exhibits an XRD pattern with two peaks belonging to the crystalline structure at 10° and 20° (Figure 5a). The amorphous pattern at 10° is because of crystalline form I, which is more hydrated and softer, while the strong pattern at 20° is because of less hydrated and harder crystalline form II, which contains hydrated crystals with incorporated water molecules in the crystal lattice. These phases are characterized by the development of crystallinity in chitosan matrices because of the formation of hydrogen bonds between chains [63, 64].

Leceta et al. [63] found that the peak at 10° disappeared with a high temperature in chitosan films produced at room temperature and 105°C. The XRD pattern of silanized hBN is presented in Figure 5b. The hBN crystalline phase exhibited a strong peak at ~26°. Additional peaks corresponding to functionalized groups were not detected. The high detection limit of the XRD device, coupled with the low VTS ratio, likely accounts for the non-detection of peaks associated with functional groups. In the study, the films produced at 50°C resulted in the observation of a small crystalline form I peak in the pure chitosan film at 10°, and the detection of a peak belonging to hBN at 26.1°. Since the amount of hBN added is max 0.9%, the peak intensity is very low. With the addition of hBN, there was a noticeable decrease in the peak intensity of chitosan. This can be attributed to the fact that the addition of hBN reduces the inclusion of hydrogen bonds in the crystal lattice in the chitosan matrix, reducing its crystallinity. Previous studies have reported an electrostatic interaction between chitosan and hBNNS without H bonding [37, 65]. In contrast to these studies, the silanization of hBN may suggest a potential bonding mechanism with chitosan involving hydrogen bonds. Spirk et al. [62] showed that silane is not only covalently bonded with the amine groups of chitosan but also via hydrogen bonding. In the FTIR spectra of all samples (Figure 4b), the decrease in the intensity of a broad absorption band in the range of 3200 to 3550 cm^{-1} consisting of N—H stretching and O—H stretching due to the overlapping of the hydroxyl group and amino group stretching vibration with the addition of hBN was also supported by the XRD pattern and revealed evidence of binding by hydrogen bonds. Figure 6 illustrates the potential binding mechanism between hBN and chitosan through hydrogen bonding. The possible mechanism is that, under acidic conditions, the amine group of chitosan protonates to form NH3+ ion and provides a suitable environment for hydrogen bonding, as suggested by Spirk et al.

3.2 | Thermal Characterization

Figure 7a show the TG curves of the samples from the thermal analysis performed under N_2 atmosphere. For each film sample, the curves depicting three-stage decomposition were observed. Because of absorbed moisture, the sample experienced water loss, and we detected the first weight loss around 150°C. This weight loss is around ~11%. The second weight loss, the largest at 240°C–350°C, can be attributed to the deacetylation and depolymerization of chitosan and the decomposition of etheric groups, glucosamine moieties, and ring-opening reactions [24]. The third weight loss above 400°C was because of residual decomposition reactions. With increasing hBN addition, the decomposition curves shifted to higher temperatures [37, 38]. Above 200°C, the total chitosan film showed a weight loss of 46.09 wt%, while the S-0.9 sample containing 0.9% hBN showed a weight loss of 44.87%. The prevention of loss through pyrolysis or volatilization results from increased chitosan retention [37]. The area of the main peak in the DTG curves of the film samples was calculated [66] and found to be 250.95, 202.25, 149.18, and 179.16 mg in samples S-0, S-0.3, S-0.6, and S-0.9, respectively. A large area under the peak indicates a more significant mass loss, which indicates a lower thermal stability, while a smaller area may indicate that the material is more stable. The lowest area was seen in sample S-0.6. In addition, the amount of residue increased with increasing hBN content [40]. When the half-weight degradation (T_{50}) temperatures were examined, the S-0 sample exhibited a

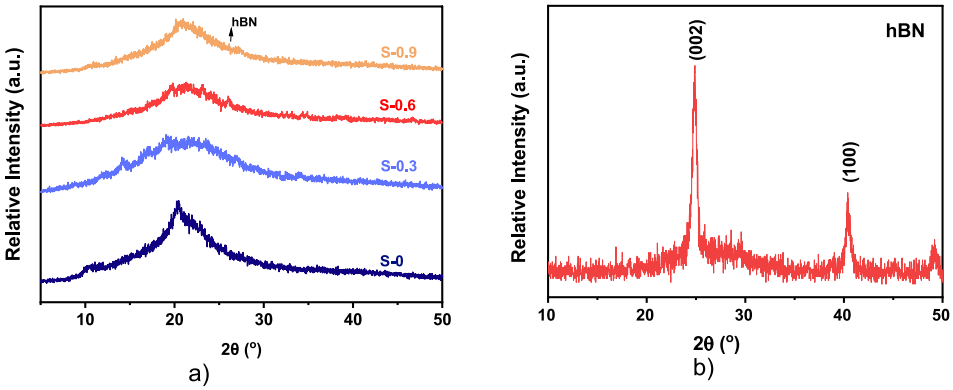

FIGURE 5 | XRD patterns of (a) the samples and (b) silanized hBN. [Color figure can be viewed at wileyonlinelibrary.com]

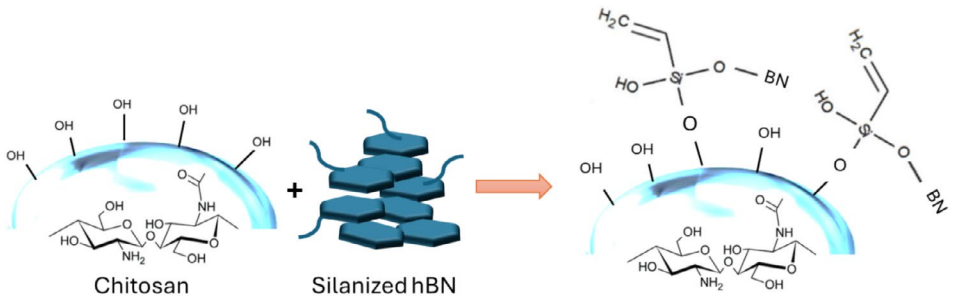

FIGURE 6 | The binding mechanism between hBN and chitosan. [Color figure can be viewed at wileyonlinelibrary.com]

T50 of 360°C, while the S-0.6 sample exhibited a T_{50} of 420°C, the most delayed among the films. Results are consistent with area calculations and the literature [67]. DTG curves of the film samples are shown in Figure 7b. The DTG results show that the interaction of hBN with chitosan can efficiently improve the thermal stability and that the thermal decomposition temperature of the films increased from 237.5°C in the S-0 sample to 248.7°C in the S-0.9 film [37]. The results obtained clearly show that incorporating hBN has a significant impact on the degradation rate of chitosan films and enhances their thermal stability.

3.3 | Properties of Films

The physical and barrier properties of food packaging are influenced by the swelling ratio and moisture binding ability, which are important factors to consider [47]. The swelling behavior is caused by the diffusion of water molecules into voids in the polymeric chain network and macromolecular relaxation [38]. The swelling rate percentage exhibits a variable trend across the samples. Sample S-0 shows the highest absorption at 146.45%, while S-0.3 demonstrates a significant reduction (119.20%) and S-0.6 and S-0.9 samples show moderate absorption values (142.84% and 125.26%, respectively), as seen in Table 1. This fluctuation suggests that the hBN addition affects the water uptake, potentially due to changes in the surface properties of the material. The swelling rate decreased with the addition of hBN, which is thought to be because of the hydrophobic nature of hBN, and similar studies have reported that hBN-added composites reduce water adsorption [38]. The equilibrium moisture content (MC) values of samples were measured at 11.76%, 13.26%, 12.71%, and 13.50%, respectively. The moisture content increases slightly with the addition of hBN. When standard deviations are considered, the values did not change significantly and were lower than in the study in which BNNP was included in chitosan [38]. Due to its structure, hBN does not exhibit swelling behavior when in contact with water; however, it can retain moisture on its surface. Therefore, the swelling amount is expected to decrease while the moisture retention ability increases with the addition of hBN to the films. It has been determined that the change is not linear depending on the hBN amount. The swelling and moisture retention behavior of the S-0.6 sample, similar to virgin S-0, suggests that a homogeneous distribution is not achieved within the structure (Figure 12c). It

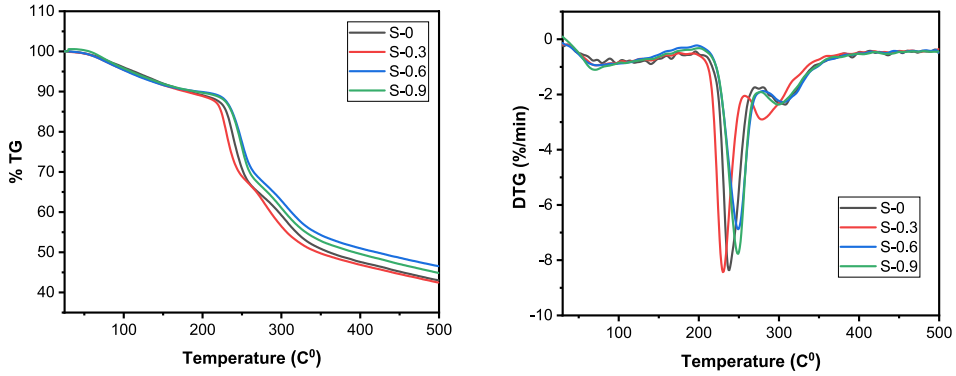

FIGURE 7 | The thermal analysis of the samples in N_2 atmosphere: (a) TGA and (b) DTG. [Color figure can be viewed at wileyonlinelibrary.com]

TABLE 1 | The swelling ratio, equilibrium moisture content, water vapor permeability, color measurement, oxygen permeability, and opacity of the samples.

	Samples			
Properties	**S-0**	**S-0.3**	**S-0.6**	**S-0.9**
Water absorption%	146.45 ± 5	119.20 ± 14	142.84 ± 16	125.26 ± 35
MC%	11.76 ± 0.52	13.26 ± 0.17	12.71 ± 1.60	13.50 ± 1.52
WVP ($\times 10^{-10}$ g^{-1} s^{-1} Pa^{-1})	2.54 ± 0.04	2.00 ± 1.12	1.76 ± 0.06	1.47 ± 0.40
L	32.86	41.075	46.735	50.09
a	−0.66	−1.62	−2.26	−2.865
b	1.725	7.125	9.17	8.345
ΔE	—	9.88	15.83	18.59
Oxygen transmission rate (mL m^{-2} day^{-1})	1350.79	542.2	1250.8	874.2
Opacity (Abs600/mm)	0.67	1.40	1.69	2.32

is thought that the undesirable agglomeration of hBN in the S-0.6 sample causes the surface area to decrease, thus preventing the expected increase in the moisture retention ability of the polymer within the film.

In a study by Jara et al. [47], the ability of a film to keep water was associated with the presence of hydrophilic groups such as carboxylic and hydroxyl groups that can easily interact with water. Glycerol has been reported to increase the swelling rates of the samples because of its hydrophilic structure. In this study, despite producing films similar to the study by Behera et al. [38] and using glycerol, MC and swelling ratio were lower. Different crosslinking processes with sodium sulfate and the use of nano-sized silanized hBN are believed to account for the lower MC and swelling ratio. The absence of N—H stretches in the FTIR spectra in Figure 4a after the crosslinking process and the decrease in the band intensity between 3200 and 3550 cm^{-1} consisting of O—H stretches showed that the crosslinking between sodium sulfate and chitosan occurred effectively. The crosslinking may limit the penetration of water molecules because of the formation of the reticulated structure of the chitosan chains. Another reason could be the interaction of hBN with the hydroxyl groups of chitosan, which may reduce the interaction of hydroxyl groups [67, 68]. This is thought to be effective in reducing the swelling rate. Additionally, this result provides further evidence that hBN bonds with covalent and H bonds because of the silanization process, as supported by XRD and FTIR results.

WVP barriers for food packaging materials are important for slowing microbial growth and increasing the storage life of packaged foods. The WVP values of S-0, S-0.3, S-0.6, and S-0.9 samples were determined as $2.54\times10^{-10}\,g^{-1}\,s^{-1}\,Pa^{-1}$, $2\times10^{-10}\,g^{-1}\,s^{-1}\,Pa^{-1}$, $1.76\times10^{-10}\,g^{-1}\,s^{-1}\,Pa^{-1}$ and $1.47\times10^{-10}\,g^{-1}\,s^{-1}\,Pa^{-1}$, respectively. The decrease in WVP of samples with increasing hBN content is because of the physical barrier created by the plate structure of hBN, which provides a tortuous path for water vapor molecules [69]. Behera et al. [34] and Kaya et al. [36] reported similar behavior for the decrease in WVP of chitosan-BNNP nanocomposites. The literature reports a WVP value of $4\times10^{-10}\,g^{-1}\,s^{-1}\,Pa^{-1}$ for the sample dried at 40°C containing 1% chitosan and 0.3% glycerol [47]. In a different study, a WVP value of $1.84\,10^{-10}\,g^{-1}\,s^{-1}\,Pa^{-1}$ was measured for chitosan containing 1% glycerol [70]. The obtained films are believed to exhibit enhanced suitability for acting as a barrier against environmental conditions and reducing water loss in packaging materials, particularly with the addition of hBN.

Table 1 shows the oxygen permeability of the film samples. Oxygen permeability value is an important parameter for long-term storage of food products without spoilage. The oxygen permeability rate of the samples varies between OTR 542.2–1350.79 $cm^3\,m^{-2}\,day^{-1}$. The oxygen permeability value in pure chitosan is higher than in composite films. The addition of hBN to the composite films led to a low flow rate. Sample S-0.3 exhibited the lowest oxygen permeability value. The reason behind the decrease in oxygen permeability when hBN is added is attributed to the layered structure of hBN [38]. The diffusion energy required for gas to pass through a high crystallinity film is higher than that of a non-crystalline film. For this reason, hBN crystals are thought to reduce the oxygen permeability of the film. The S-0.6 sample showed increased permeability, while the S-0.9 sample exhibited a decrease. The literature contains studies that show a pattern of initial increase, followed by a reduction in gas permeability values when incorporating hBN into various composite films [71]. Leceta et al. [72] showed that oxygen permeability increased with the addition of glycerol. Researchers reported that the plasticizing effect of glycerol increases the mobility of the chains and facilitates the diffusion of oxygen molecules through the film. Although glycerol was used in the study, the result was lower than the 5313 $cm^3\,m^{-2}\,day^{-1}$ OTR value measured by Jančič et al. [73] for pure chitosan without glycerol.

The measured L, a, b color parameters of the films are presented in Table 1, while the digital photographs can be observed in Figure 8c. Color measurements were performed without reference on the back of the films. The ΔE values exhibited a positive correlation with the concentration of hBN in the samples. Given the opaqueness of hBN, the addition in the chitosan film caused a rise in the color parameters observed in the samples. The film samples' transparency was measured by a UV spectrophotometer in the wavelength range of 200 to 850 nm. Table 1 shows the opacity values of the films calculated using Equation (1) at 600 nm wavelength. The opacity increased because of the addition of hBN compared to pure chitosan. This result showed that the addition of hBN inhibited the cross of light through the chitosan film. Figure 8a shows the UV transmittance graph of the films. The transmittance values of the pure chitosan film are higher than the composites at all wavelengths. This makes it appear very transparent to the naked eye (Figure 8c). It is expected that hBN, which offers a strong light absorption in the UV band, will result in an efficient blockage of UV light [37]. As expected, the light transmittance values of the films decreased and UV resistance increased with the addition of hBN. UV-absorbent films have the potential to serve as a solution for packaging and extending the shelf life of food products that are sensitive to oxidative rancidity catalyzed by UV light [24]. The result shows that adding hBN can extend the shelf life of foods in packaging products. Additionally, it was observed that the transmittance values of all samples were lower in the UV light (190–400 nm) region compared to the visible light (400–760 nm) range. The results found in the study are compatible with the studies of BNNS and BNNP added chitosan films by Wang [37] and Behera et al. [38], respectively.

Figure 8b shows the blocking effect of the film samples in the UV-B region at 300 nm and in the visible regions at 700 and 750 nm. The increase in the amount of hBN led to a significant decrease in UV and visible light transmittance. In the literature, the blocking effect in the sample containing 1% BNNP is around 60 in the UV region at 300 nm, while it is around 25–30 in the visible range at 700 and 750 nm [38]. In this study, the blocking effect of the film containing 0.9% hBN is below 25 both in the UV 300 nm and in the visible light range of 700 and 750 nm. These findings suggest that the prepared films display a stronger ability to block UV radiation. All the results show that hBN-doped composites improve the UV barrier properties compared to pure chitosan films. This makes them appropriate packaging materials for protecting UV-sensitive products, such as food and pharmaceuticals, from UV degradation. The

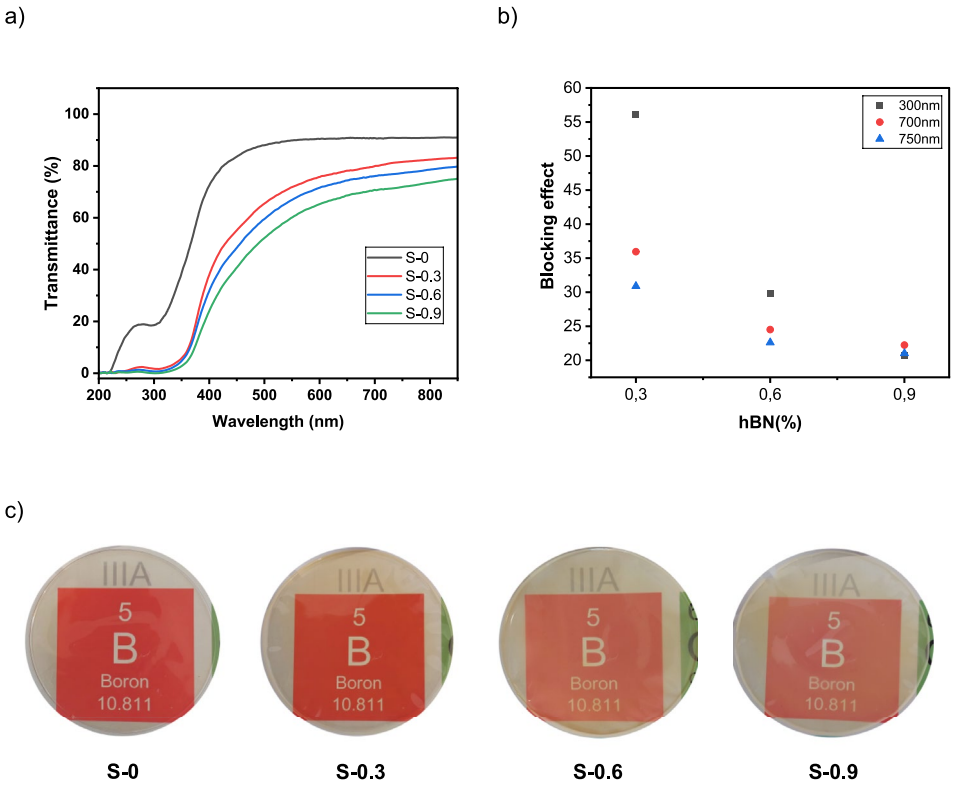

FIGURE 8 | (a) The UV transmittance graph, (b) the blocking effect, and (c) the digital photographs of samples. [Color figure can be viewed at wileyonlinelibrary.com]

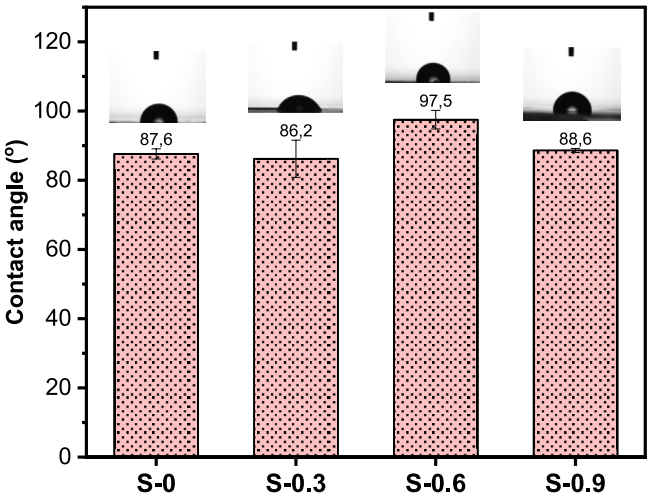

FIGURE 9 | Contact angles of the samples. [Color figure can be viewed at wileyonlinelibrary.com]

digital photographs of the films in Figure 8c clearly depict the changes in color and opacity resulting from the increasing addition of hBN. The visuals confirm the L, a, b color parameters of the films.

Contact angle values of the specimens are given in Figure 9. When the results are analyzed, 87.60 ± 1.47, 86.23 ± 5.37, 97.59 ± 2.68, and 88.62 ± 0.59 o values were found for S-0, S-0.3, S-0.6, and S-0.9 samples, respectively. The S-0.6 sample exhibited the highest value, whereas the S-0.3 sample showed a decrease in value compared to pure chitosan. The reduction can be disregarded due to the alteration in the standard deviation. In other samples, the contact angle increased with the addition of hydrophobic hBN. This shows that the hydrophobic value increases and is useful for the production of water-resistant packaging in the packaging industry. The change toward the increase in the contact angle with the addition of hBN is consistent with the studies [37, 38, 67]. The increase in contact angles is believed to have a positive impact on the water vapor barrier capacity, and this notion is reinforced by the observed decrease in WVP values [37].

3.4 | Chemical Resistance Properties

The weight losses of the film samples at weekly time intervals after treatment with NaOH for up to 10 weeks are shown in Figure 10. A calculation was performed to determine the chemical degradation rate of the S-0, S-0.3, S-0.6, and S-0.9 samples in a 1 M NaOH solution over 10 weeks, yielding values of 17.02%, 18.71%, 17.29%, and 18.93%, respectively. The difference in chemical degradation between the composite film with the highest hBN addition (S-0.9) and pure chitosan was observed at 1.91%. According to Takara et al. [74], the treatment of chitosan films with NaOH at different concentrations induced deprotonation, extraction of phosphate, and elevated CH deacetylation, which facilitated the formation of new hydrogen bonds. These studies also reported that the reduction of new hydrogen bonds and N-acetyl groups reduced the swelling properties by producing films with a more compact and irregular structure. hBN may have reduced the formation of this compact structure. However, these rates do not have a detrimental impact on the properties of

the films. The values of the standard deviation indicate a high level of similarity among them.

3.5 | Mechanical Properties

The effect of hBN addition on the mechanical properties of chitosan was investigated by tensile tests. The results are reported in Figure 11. Depending on the amount of hBN added, an increase in tensile strength and Young's modulus was observed after a sudden decrease when compared to virgin chitosan films. This trend is observed because of the increase in the amount of BN, similar to the studies of Behera et al. [38] 1% boron nitride nanosheet added chitosan films had a TS value of 74 MPa and a YM value of 956 MPa. Wang et al. [37] found that the TS value of chitosan films with 1% BNNS addition was ~25 MPa. In this study, the TS value of the sample containing 0.9% hBN was 77.9 MPa (Figure 11a) and the YM value was 6299.86 MPa (Figure 11b). Unlike these studies, the glycerol used in this study provides an advantage because of the improvement in the flexibility of thin film materials, as it reduces the intermolecular forces between polymer chains and increases the free volume [70]. Additionally, the enhancement in mechanical properties with increasing hBN addition can be attributed to the electrostatic interaction between hBN and chitosan, which increases the strength [37]. This proves that the mechanical properties are affected by the production method, and the method used in the study was successful.

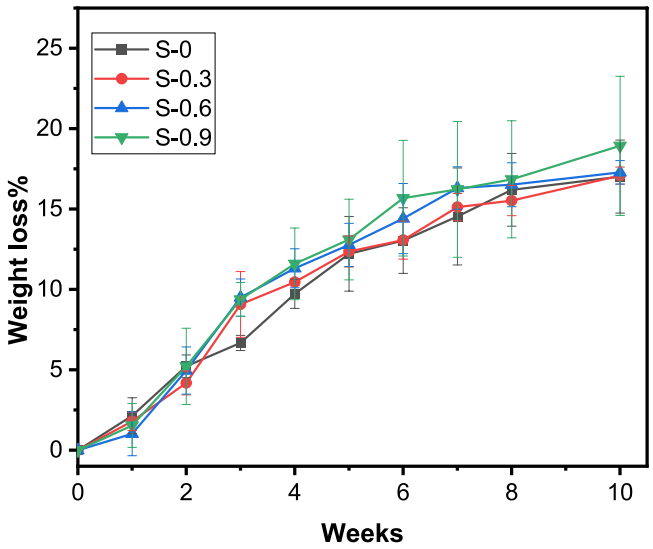

FIGURE 10 | The percent weight loss of the samples in NaOH solution depending on the weekly waiting time. [Color figure can be viewed at wileyonlinelibrary.com]

SEM images of composite films containing pure chitosan and hBN are shown in Figure 12. The images on the left side of the samples were taken from the flat surface, and the images on the right side were taken from the rupture surfaces of the fragments that broke off as a result of the tensile test. The hBN agglomerates were observed in the S-0.6 sample (Figure 12c). While Hammi et al. [67] stated in their study that agglomerations may occur in certain regions as a result of hBN agglomeration in preparing composite films, a similar result was also observed in graphene-chitosan films [75]. The chitosan film exhibited brittle fracture behavior in the tensile direction, with lines/bands radiating in a certain direction (Figure 12a) [76]. It was determined that as the amount of hBN increased, it had a smooth surface and hBN agglomerates in some regions. This phenomenon indicates that the interfacial adhesion between chitosan and hBN is enhanced in these compositions. In the regions where agglomerates are located, parabolic-shaped depressions characteristic of ductile fracture formed under the effect of shear stress were observed (Figure 12b,c) [77, 78]. The observed aggregates in the S-0.3 and S-0.6 samples are believed to have been responsible for the decline in mechanical properties. SEM observations explained the change in mechanical properties as a result of the tensile test, and that it exhibited brittle fracture behavior according to the tensile direction with increasing hBN showed that it was important to add the appropriate amount of filler to the matrix.

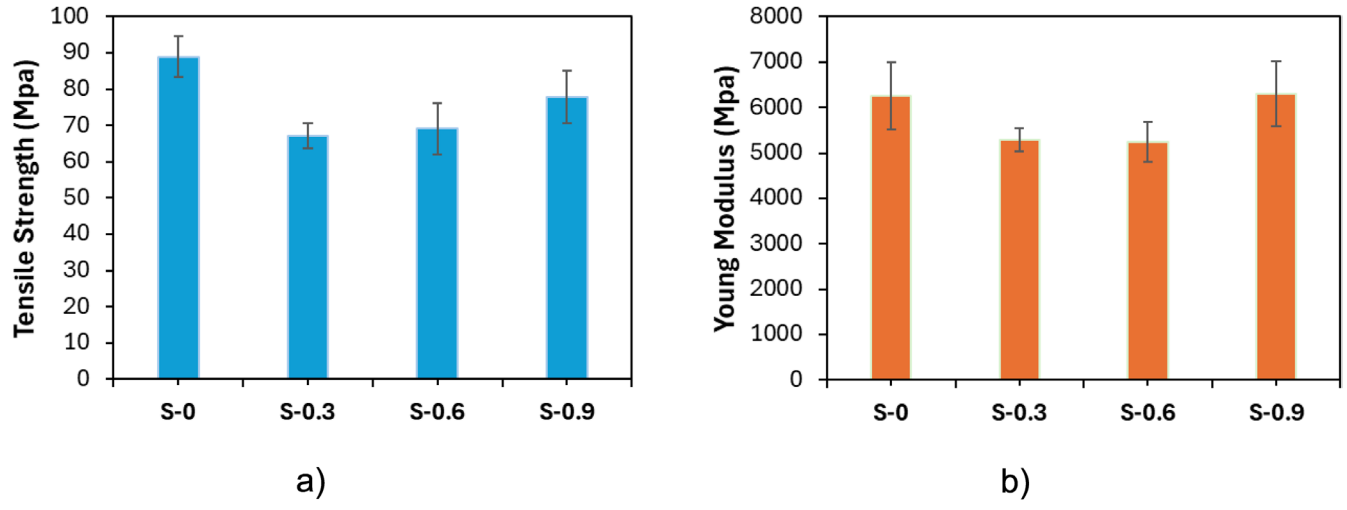

FIGURE 11 | Mechanical properties of the specimens (a) Tensile strength and (b) Young's modulus. [Color figure can be viewed at wileyonlinelibrary.com]

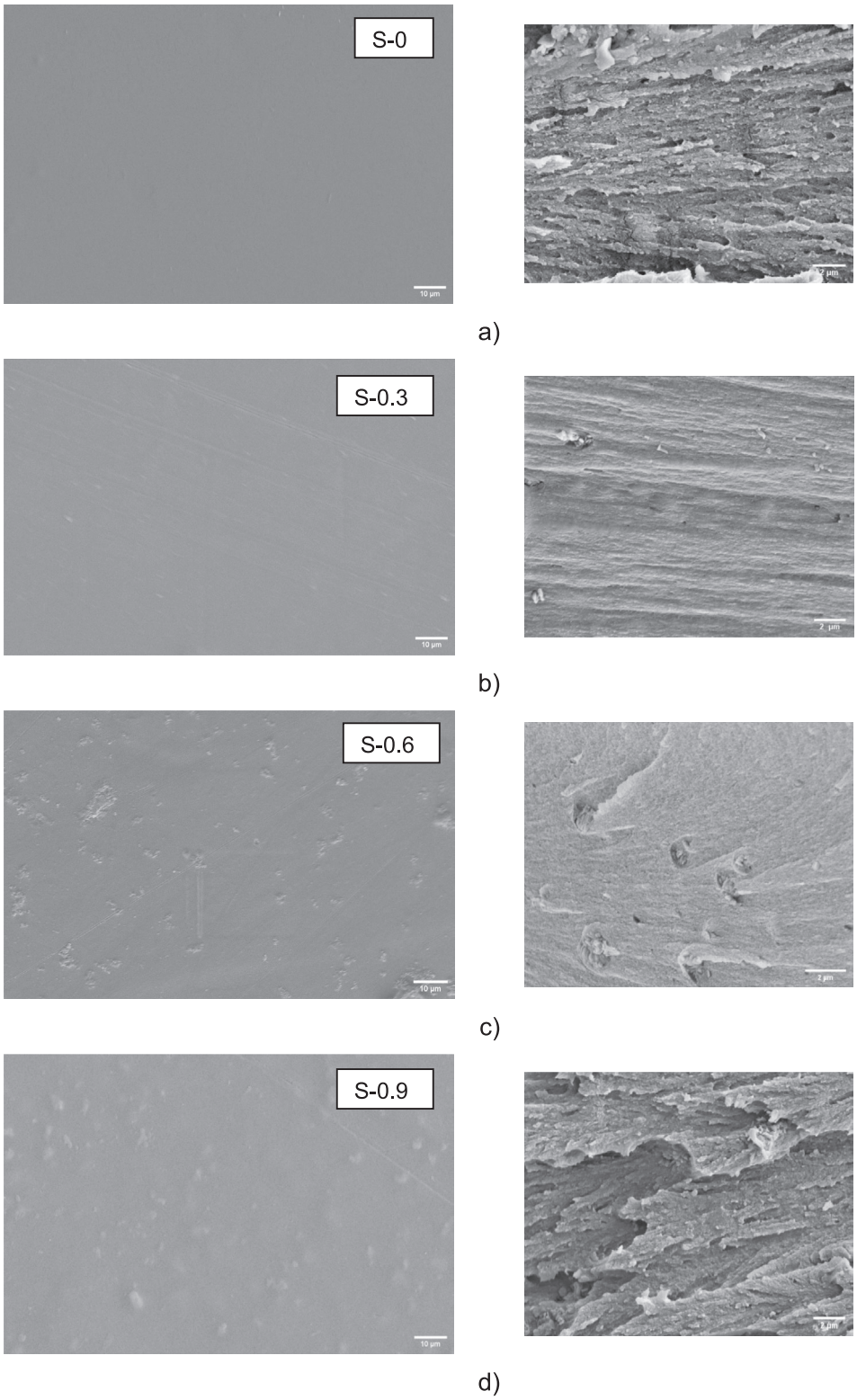

FIGURE 12 | SEM image of the samples.

3.6 | Cytotoxicity Results

Cytotoxicity tests were performed using the L929 cell line at three different time points, 24, 48, and 72 h, at five different concentrations, each with three replicates. As a result of the experiments, the viability data given in Figure 13 were obtained. Low cytotoxicity results are necessary to minimize health risks for food packaging material. When the viability rates of the samples at the 24th hour in Figure 13a are examined, cell viability is higher at all concentrations in the hBN-added samples compared to the pure chitosan sample. In the 48th and 72nd hour controls, the cell viability of the hBN-added samples at low

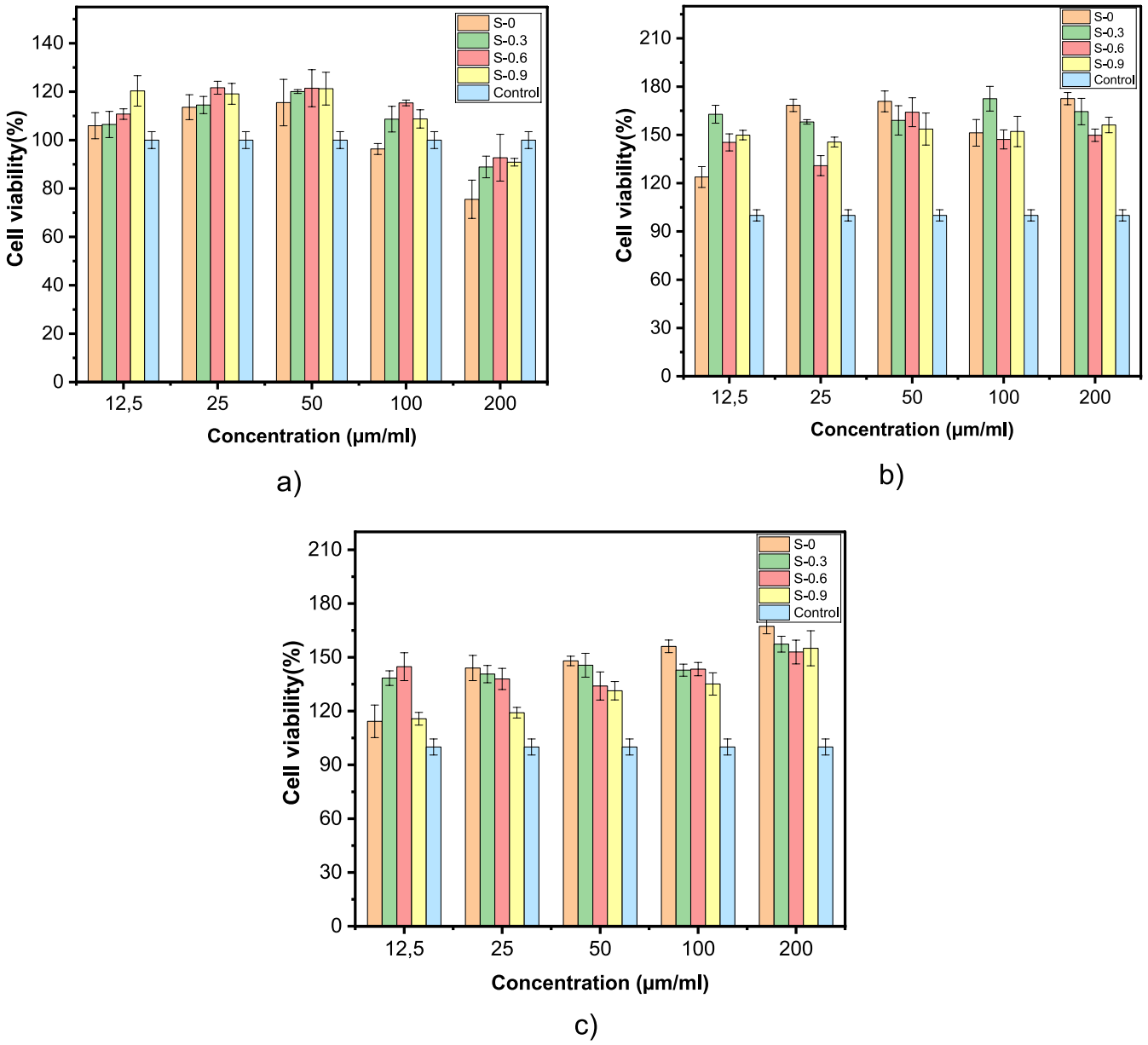

FIGURE 13 | Mean percent viability values (a) after 1 day (24 h) (b) after 2 days (48 h) (c) after 3 days (72 h). [Color figure can be viewed at wileyonlinelibrary.com]

concentrations generally increased slightly compared to chitosan, and some decrease in viability was observed at increasing concentration values. For the S-0.9 sample, at the highest cell concentration of 200 $\mu g\,mL^{-1}$, the decrease was found to be 9.48% for 48 h and 7.31% for 72 h compared to chitosan. This agrees with the study conducted by Behera et al. [38]. However, the percentage of viability is higher than the positive control. This shows that the addition of hBN increases cell viability. The changes according to hBN concentration are very close to each other and do not adversely affect the composite cytotoxicity. Although some decrease in viability rates was observed because of the increase in cell line concentration and time, it did not fall below the positive control values. The results are consistent with the studies investigating the effects of hBN on cell anti-microbial and cell viability [22, 23]. It has been shown that cell viability of hBN-added chitosan composites was observed, biocompatibility was good, and no toxic effect was observed.

4 | Conclusion

Chitosan films were successfully prepared with hBN acting as a nano filler. The conclusion reached was that the addition of hBN after silanization resulted in the formation of hydrogen bonds with chitosan. Crosslinking was provided with sodium sulfate. The addition of hBN shifted the degradation curves of the films to higher temperatures and increased the thermal stability. The addition of silanized hBN suggests that it may contribute to a more opaque material and potentially affect the light-blocking properties of the material. Furthermore, UV barrier properties were found to be improved by hBN-added composites. The gradual decrease in water vapor permeability suggests that silanized hBN can improve the barrier properties of the polymer, potentially making it more resistant to moisture transfer. The reduction in oxygen transmission rate with the addition of silanized hBN improves its resistance to oxygen permeation, which can increase its

durability and performance in various applications. Although the resistance of the composite films to NaOH decreased slightly, it is not at a level to create a negative effect. When the composite films were compared with pure chitosan film, there was a decrease in mechanical properties, but an improvement trend was observed as the hBN ratio increased. In composite films, cell viability at all concentrations and time periods is above the positive control value. The results showed that hBN-added chitosan composites exhibited good biocompatibility and no toxic effect. The obtained results show that hBN-added chitosan films have various improved physical properties, low UV and oxygen permeability, and are non-toxic. This study shows that the films produced have the potential to serve as packaging materials for safeguarding UV, oxygen, and moisture-sensitive products. The enhanced composite properties resulting from hBN addition to chitosan are highly significant for the packaging sector today, where environmentally friendly materials are in demand due to their superior properties, durability during use, and biodegradability. This material offers great potential for use, especially for food packaging. Future studies are focused on investigating and analyzing the actual effect of the prepared composite film in different application scenarios (e.g., meat, fruit, vegetable preservation, etc.), and research on the biodegradability and environmental impact of materials.

Author Contributions

Zuhal Yılmaz: conceptualization (equal), data curation (equal), formal analysis (equal), funding acquisition (supporting), investigation (lead), methodology (equal), project administration (equal), resources (equal), software (equal), supervision (equal), validation (equal), visualization (equal), writing – original draft (equal), writing – review and editing (equal). **Yapıncak Göncü:** formal analysis (equal), methodology (equal), software (equal), validation (equal), visualization (equal), writing – original draft (equal), writing – review and editing (equal). **Nuran Ay:** conceptualization (lead), funding acquisition (equal), methodology (lead), resources (equal), supervision (lead), validation (lead), writing – original draft (lead), writing – review and editing (lead).

Acknowledgments

The authors would like to thank the financial support from the Scientific Research Project Commission of Eskişehir Technical University (grant numbers: 22GAP257), and Assoc. Prof. Zerrin Günkaya from the Department of Environmental Engineering at Eskişehir Technical University for oxygen permeability measurements.

Ethics Statement

The authors have nothing to report.

Conflicts of Interest

The authors declare no conflicts of interest.

Data Availability Statement

The data that support the findings of this study are available from the corresponding author upon reasonable request.

References

1. B. Nowak, J. Pajk, and J. Karcz, "Biodegradation of Pre-Aged Modified Polyethylene Films," in *Scanning Electron Microscopy* (InTech, 2012), https://doi.org/10.5772/35128.

2. P. M. Trivedi, C. P. Gocher, V. Balachandran, and V. K. Gupta, "Insight of Polypropylene Synthesis With High Performance Multidentate Internal Donor Catalyst System," *Journal of Applied Polymer Science* 140, no. 11 (2023): e53609, https://doi.org/10.1002/APP.53609.

3. A. Sebastian, R. Gopika, R. Anju, M. Verma, and M. T. Ramesan, "Improvement in Structural, Thermal, Charge Transport and Mechanical Properties of Poly (Methyl Methacrylate)/Polyindole Composites for Optoelectronic Devices," *Physica Scripta* 98 (2023): 6, https://doi.org/10.1088/1402-4896/ACCFC7.

4. S. S. Furhan, and M. T. Ramesan, "Structural, Conductivity, Mechanical and Wettability Properties of Copper Alumina Reinforced Chlorinated Polyethylene/Polyvinyl Chloride Blend Nanocomposites," *Research on Chemical Intermediates* 49, no. 5 (2023): 1891–1908, https://doi.org/10.1007/S11164-022-04881-9.

5. S. van Hurne, S. K. Raut, and M. M. J. Smulders, "Recyclable Covalent Adaptable Polystyrene Networks Using Boronates and TetraAzaADamantanes," *ACS Applied Polymer Materials Journal* 6, no. 13 (2024): 7918–7925, https://doi.org/10.1021/ACSAPM.4C01633.

6. H. S. Kim, H. J. Kim, J. W. Lee, and I. G. Choi, "Biodegradability of Bio-Flour Filled Biodegradable Poly(Butylene Succinate) bio-Composites in Natural and Compost Soil," *Polymer Degradation and Stability* 91, no. 5 (2006): 1117–1127, https://doi.org/10.1016/j.polymdegradstab.2005.07.002.

7. K. Behera, Y. H. Chang, F. C. Chiu, and J. C. Yang, "Characterization of Poly(Lactic Acid)s With Reduced Molecular Weight Fabricated Through an Autoclave Process," *Polymer Testing* 60 (2017): 132–139, https://doi.org/10.1016/j.polymertesting.2017.03.015.

8. Y. Tokiwa and B. P. Calabia, "Biodegradability and Biodegradation of Polyesters," *Journal of Polymers and the Environment* 15, no. 4 (2007): 259–267, https://doi.org/10.1007/s10924-007-0066-3.

9. M. Rinaudo, "Chitin and Chitosan: Properties and Applications," *Progress in Polymer Science* 31, no. 7 (2006): 603–632, https://doi.org/10.1016/j.progpolymsci.2006.06.001.

10. A. Muxika, A. Etxabide, J. Uranga, P. Guerrero, and K. de la Caba, "Chitosan as a Bioactive Polymer: Processing, Properties and Applications," *International Journal of Biological Macromolecules* 105 (2017): 1358–1368, https://doi.org/10.1016/j.ijbiomac.2017.07.087.

11. L. Bedian, A. M. Villalba-Rodríguez, G. Hernández-Vargas, R. Parra-Saldivar, and H. M. N. Iqbal, "Bio-Based Materials With Novel Characteristics for Tissue Engineering Applications – A Review," *International Journal of Biological Macromolecules* 98 (2017): 837–846, https://doi.org/10.1016/j.ijbiomac.2017.02.048.

12. J. Lizardi-Mendoza, W. M. Argüelles Monal, and F. M. Goycoolea Valencia, "Chemical Characteristics and Functional Properties of Chitosan," in *Chitosan in the Preservation of Agricultural Commodities* (Academic Press, 2016), 3–31, https://doi.org/10.1016/B978-0-12-802735-6.00001-X.

13. A. Verlee, S. Mincke, and C. V. Stevens, "Recent Developments in Antibacterial and Antifungal Chitosan and Its Derivatives," *Carbohydrate Polymers* 164 (2017): 268–283, https://doi.org/10.1016/j.carbpol.2017.02.001.

14. L. J. Bastarrachea, D. E. Wong, M. J. Roman, Z. Lin, J. M. Goddard, and S. Farris, "Active Packaging Coatings," *Coatings* 5 (2015): 771–791, https://doi.org/10.3390/coatings5040771.

15. J. H. HanInnovation, *Food Packaging*, Second ed. (Elsevier, 2014).

16. M. Mujtaba, R. E. Morsi, G. Kerch, et al., "Current Advancements in Chitosan-Based Film Production for Food Technology; A Review," *International Journal of Biological Macromolecules* 121 (2019): 889–904, https://doi.org/10.1016/j.ijbiomac.2018.10.109.

17. S. K. Swain, S. Dash, S. K. Kisku, and R. K. Singh, "Thermal and Oxygen Barrier Properties of Chitosan Bionanocomposites by Reinforcement of Calcium Carbonate Nanopowder," *Journal of Materials Science*

and Technology 30, no. 8 (2014): 791–795, https://doi.org/10.1016/j.jmst.2013.12.017.

18. X. Zhang, Y. Liu, H. Yong, Y. Qin, J. Liu, and J. Liu, "Development of Multifunctional Food Packaging Films Based on Chitosan, TiO_2 Nanoparticles and Anthocyanin-Rich Black Plum Peel Extract," *Food Hydrocolloids* 94 (2019): 80–92, https://doi.org/10.1016/j.foodhyd.2019.03.009.

19. H. Wu, "Effect of Citric Acid Induced Crosslinking on the Structure and Properties of Potato Starch/Chitosan Composite Films," *Food Hydrocolloids* 97 (2019): 105208, https://doi.org/10.1016/j.foodhyd.2019.105208.

20. K. Meera and M. T. Ramesan, "Tailoring the Performance of Boehmite Nanoparticles Reinforced Carboxymethyl Chitosan/Cashew Gum Blend Nanocomposites via Green Synthesis," *Polymer (Guildf)* 268 (2023): 125706, https://doi.org/10.1016/J.POLYMER.2023.125706.

21. M. S. Baskar, Sooryajayan, A. J. Kalladi, B. K. Bahuleyan, and M. T. Ramesan, "Development of High Strength, Thermal Resistant and Electrical Properties of Polyindole/Carboxymethyl Chitosan/Alumina Blend Nanocomposites for Flexible Energy Storage Applications," *Emergent Materials* 7, no. 3 (2024): 887–898, https://doi.org/10.1007/S42247-024-00629-W.

22. M. Kıvanç, B. Barutca, A. T. Koparal, Y. Göncü, S. H. Bostancı, and N. Ay, "Effects of Hexagonal Boron Nitride Nanoparticles on Antimicrobial and Antibiofilm Activities, Cell Viability," *Materials Science and Engineering: C* 91 (2018): 115–124, https://doi.org/10.1016/J.MSEC.2018.05.028.

23. A. Merlo, V. R. S. S. Mokkapati, S. Pandit, and I. Mijakovic, "Boron Nitride Nanomaterials: Biocompatibility and Bio-Applications," *Biomaterials Science* 6, no. 9 (2018): 2298–2311, https://doi.org/10.1039/C8BM00516H.

24. A. Mukheem, S. Shahabuddin, N. Akbar, et al., "Boron Nitride Doped Polyhydroxyalkanoate/Chitosan Nanocomposite for Antibacterial and Biological Applications," *Nanomaterials* 9, no. 4 (2019): 1–14, https://doi.org/10.3390/nano9040645.

25. S. Pandit, K. Gaska, V. R. S. S. Mokkapati, et al., "Antibacterial Effect of Boron Nitride Flakes With Controlled Orientation in Polymer Composites," *RSC Advances* 9, no. 57 (2019): 33454–33459, https://doi.org/10.1039/c9ra06773f.

26. A. T. Seyhan, A. Tuna, O. Durukan, Y. Göncü, S. Turan, and N. Ay, "Creep and Recovery Behaviors of Chemically Induced Grafted Low Density Polyethylene Films Containing Silanized Hexagonal Boron Nitride Nanosheets," *Materials Express* 8 (2018): 55–67, https://doi.org/10.1166/mex.2018.1404.

27. A. Akay, O. Durukan, Y. Göncü, A. T. Seyhan, and N. Ay, "Hexagonal Boron Nitride Filled Polymer Nanofibers Producing and Characterization via Electrospinning Technique," *Usak University Journal of Material Sciences* 1 (2012): 35–41.

28. M. R. Miah, J. Ding, H. Zhao, et al., "Boron Nitride-Based Polyester Nanocomposite Films With Enhanced Barrier and Mechanical Performances," *ACS Applied Polymer Materials Journal* 6, no. 5 (2024): 2913–2923, https://doi.org/10.1021/ACSAPM.3C03148.

29. M. Seth and S. G. Hatzikiriakos, "Combining Boron Nitride With a Fluoroelastomer: An Enhanced Polymer Processing Additive," *Journal of Vinyl & Additive Technology* 7, no. 2 (2001): 90–97, https://doi.org/10.1002/VNL.10273.

30. S. G. Hatzikiriakos, "Boron Nitride Based Polymer Processing Aids," *Polymer Processing Instabilities: Control and Understanding* 15 (2004): 261–285.

31. N. Rathod and S. G. Hatzikiriakos, "The Effect of Surface Energy of Boron Nitride on Polymer Processability," *Polymer Engineering and Science* 44, no. 8 (2004): 1543–1550, https://doi.org/10.1002/PEN.20151.

32. N. Ay, Y. Göncü, and G. Ay, "Bor Nitrür: Üretimi ve Uygulamalardaki Son Gelişmeler," Paper presented at *International Shymposium on Boron, Turkey*, 2019.

33. I. B. Kazatchkov, F. Yip, and v. S. G. Hatzikiriakos, "The Effect of Boron Nitride on the Rheology and Processing of Polyolefins," *Rheologica Acta* 39, no. 6 (2000): 583–594, https://doi.org/10.1007/s003970000113.

34. M. Emanet, E. Kazanç, Z. Çobandede, and v. M. Çulha, "Boron Nitride Nanotubes Enhance Properties of Chitosan-Based Scaffolds," *Carbohydrate Polymers* 151 (2016): 313–320, https://doi.org/10.1016/j.carbpol.2016.05.074.

35. S. Dhanavel, "Cross-Linked Chitosan/Hydroxylated Boron Nitride Nanocomposites for Co-Delivery of Curcumin and 5-Fluorouracil Towards Human Colon Cancer Cells," *Journal of the Iranian Chemical Society* 18, no. 2 (2021): 317–329, https://doi.org/10.1007/s13738-020-02031-9.

36. T. H. Chiang and T. E. Hsieh, "A Study of Encapsulation Resin Containing Hexagonal Boron Nitride (hBN) as Inorganic Filler," *Journal of Inorganic and Organometallic Polymers and Materials* 16, no. 2 (2006): 175–183, https://doi.org/10.1007/s10904-006-9037-8.

37. K. Wang, F. Li, X. Sun, F. Wang, D. Xie, and Y. Wei, "Transparent Chitosan/Hexagonal Boron Nitride Nanosheets Composite Films With Enhanced UV Shielding and Gas Barrier Properties," *International Journal of Biological Macromolecules* 251 (2023): 126308, https://doi.org/10.1016/j.ijbiomac.2023.126308.

38. K. Behera, M. Kumari, Y. H. Chang, and F. C. Chiu, "Chitosan/Boron Nitride Nanobiocomposite Films With Improved Properties for Active Food Packaging Applications," *International Journal of Biological Macromolecules* 186 (2021): 135–144, https://doi.org/10.1016/j.ijbiomac.2021.07.022.

39. S. N. M. Shareef, K. Chidambaram, and S. K. K. Pasha, "Structure, Morphology and Dielectric Properties of Hexagonal Boron Nitride Nanoparticles Reinforced Biopolymer Nanocomposites," *Polymer-Plastics Technology and Materials* 58 (2019): 1210–1225, https://doi.org/10.1080/03602559.2018.1542726.

40. S. K. Kisku and S. K. Swain, "Synthesis and Characterization of Chitosan/Boron Nitride Composites," *Journal of the American Ceramic Society* 95, no. 9 (2012): 2753–2757, https://doi.org/10.1111/j.1551-2916.2012.05140.x.

41. B. Kaya, N. N. Zorba, and C. Caner, "Development of Novel Biodegradable Film Based on Chitosan With Borax (Sodium Tetraborate) and Boron Nitride and Their Biological Activity," *International Journal of Food Science and Technology* 58, no. 2 (2023): 890–897, https://doi.org/10.1111/ijfs.15743.

42. L. Koroglu, E. Ayas, and N. Ay, "BNNS Formation Through Surface Modification of hBN Nanopowders With a Silane Coupling Agent," *Journal of Dispersion Science and Technology* 45, no. 8 (2023): 1562–1573, https://doi.org/10.1080/01932691.2023.2222806.

43. A. T. Seyhan, Y. Göncü, O. Durukan, A. Akay, and N. Ay, "Silanization of Boron Nitride Nanosheets (BNNSs) Through Microfluidization and Their Use for Producing Thermally Conductive and Electrically Insulating Polymer Nanocomposites," *Journal of Solid State Chemistry* 249 (2017): 98–107, https://doi.org/10.1016/j.jssc.2017.02.020.

44. M. Tanveer, A. Farooq, S. Ata, et al., "Aluminum Nanoparticles, Chitosan, Acrylic Acid and Vinyltrimethoxysilane Based Hybrid Hydrogel as a Remarkable Water Super-Absorbent and Antimicrobial Activity," *Surfaces and Interfaces* 25 (2021): 101285, https://doi.org/10.1016/j.surfin.2021.101285.

45. Z. Kalaycıoğlu, E. Torlak, G. Akın-Evingür, İ. Özen, and F. B. Erim, "Antimicrobial and Physical Properties of Chitosan Films Incorporated With Turmeric Extract," *International Journal of Biological Macromolecules* 101 (2017): 882–888, https://doi.org/10.1016/j.ijbiomac.2017.03.174.

46. M. Yadav, K. Behera, Y. H. Chang, and F. C. Chiu, "Cellulose Nanocrystal Reinforced Chitosan Based UV Barrier Composite Films for

Sustainable Packaging," *Polymers (Basel)* 12, no. 1 (2020): 1–22, https://doi.org/10.3390/polym12010202.

47. A. Homez-Jara, L. D. Daza, D. M. Aguirre, J. A. Muñoz, J. F. Solanilla, and H. A. Váquiro, "Characterization of Chitosan Edible Films Obtained With Various Polymer Concentrations and Drying Temperatures," *International Journal of Biological Macromolecules* 113 (2018): 1233–1240, https://doi.org/10.1016/j.ijbiomac.2018.03.057.

48. L. Castillo, O. López, C. López, et al., "Thermoplastic Starch Films Reinforced With Talc Nanoparticles," *Carbohydrate Polymers* 95, no. 2 (2013): 664–674, https://doi.org/10.1016/j.carbpol.2013.03.026.

49. M. Escamilla-García, M. C. García-García, J. Gracida, et al., "Properties and Biodegradability of Films Based on Cellulose and Cellulose Nanocrystals From Corn Cob in Mixture With Chitosan," *International Journal of Molecular Sciences* 23, no. 18 (2022): 10560, https://doi.org/10.3390/ijms231810560.

50. [ASTM] American Society for Testing and Materials, "Standard Test Methods for Water Vapor Transmission of Materials," in *Material Science View Project Photocatalytic View Project* (ASTM International, 2019), 1–3.

51. ISO/TC 61/SC 2 Mechanical Behavior, "Plastics — Determination of Tensile Properties — Part 2: Test Conditions for Moulding and Extrusion Plastics," Ics 83.080.01 2, s. 11 (2012).

52. D. H. A. Besisa, M. A. A. Hagras, E. M. M. Ewais, Y. M. Z. Ahmed, Z. I. Zaki, and A. Ahmed, "Low Temperature Synthesis of Nano-Crystalline h-Boron Nitride From Boric Acid/ Urea Precursors," *Journal of Ceramic Processing Research* 17, no. 12 (2016): 1219–1225.

53. J. Duan, R. Xue, Y. Xu, and C. Sun, "Low Temperature Synthesis of h-BN Nanoflakes," *Materials Letters* 62, no. 19 (2008): 3355–3357, https://doi.org/10.1016/J.MATLET.2008.03.007.

54. S. Chandra Dey and M. Al-Amin, "Preparation, Characterization and Performance Evaluation of Chitosan as an Adsorbent for Remazol Red," *International Journal of Engineering Research & Technology* 2, no. 21 (2016): 52–62.

55. K. Vijayalakshmi, B. M. Devi, P. N. Sudha, J. Venkatesan, and S. Anil, "Synthesis, Characterization and Applications of Nanochitosan/ Sodium Alginate/Microcrystalline Cellulose Film," *Journal of Nanomedicine & Nanotechnology* 7, no. 6 (2016): 1–11, https://doi.org/10.4172/2157-7439.1000419.

56. M. M. A. Al-Remawi, "Properties of Chitosan Nanoparticles Formed Using Sulfate Anions as Crosslinking Bridges," *American Journal of Applied Sciences* 9, no. 7 (2012): 1091–1100, https://doi.org/10.3844/ajassp.2012.1091.1100.

57. U. K. Parida and v. B. Kumar Bindhani, "Cross-Linked Chitosan-Sodium Sulfate Matrix Systems Using Gel Casting Method for Sustained Drug Release of Doxorubicin Hydrochloride," *International Journal of Drug Delivery* 7 (2015): 101–112.

58. N. Kahya, H. Kaygusuz, and F. B. Erim, "Aqueous Removal of Sodium Dodecyl Benzene Sulfonate (SDBS) by Crosslinked Chitosan Films," *Journal of Polymers and the Environment* 26, no. 5 (2018): 2166–2172, https://doi.org/10.1007/s10924-017-1113-3.

59. V. R. Netala, S. Bukke, L. Domdi, et al., "Biogenesis of Silver Nanoparticles Using Leaf Extract of *Indigofera hirsuta* L. and Their Potential Biomedical Applications (3-In-1 System)," *Artificial Cells, Nanomedicine, and Biotechnology* 46 (2018): 1138–1148, https://doi.org/10.1080/21691401.2018.1446967.

60. M. F. Queiroz, K. R. T. Melo, D. A. Sabry, G. L. Sassaki, and H. A. O. Rocha, "Does the Use of Chitosan Contribute to Oxalate Kidney Stone Formation?," *Marine Drugs* 13, no. 1 (2015): 141–158, https://doi.org/10.3390/md13010141.

61. R. Yokose, T. Shimasaki, N. Teramoto, and M. Shibata, "Amino Acid-Incorporated Polymer Network by Thiol-Ene Polymerization," *Express Polymer Letters* 9, no. 8 (2015): 744–755, https://doi.org/10.3144/EXPRESSPOLYMLETT.2015.69.

62. S. Spirk, G. Findenig, A. Doliska, et al., "Chitosan-Silane Sol-Gel Hybrid Thin Films With Controllable Layer Thickness and Morphology," *Carbohydrate Polymers* 93, no. 1 (2013): 285–290, https://doi.org/10.1016/j.carbpol.2012.04.030.

63. I. Leceta, P. Guerrero, I. Ibarburu, M. T. Dueñas, and K. De La Caba, "Characterization and Antimicrobial Analysis of Chitosan-Based Films," *Journal of Food Engineering* 116, no. 4 (2013): 889–899, https://doi.org/10.1016/j.jfoodeng.2013.01.022.

64. C. Pastor, L. Sánchez-González, A. Chiralt, M. Cháfer, and C. González-Martínez, "Physical and Antioxidant Properties of Chitosan and Methylcellulose Based Films Containing Resveratrol," *Food Hydrocolloids* 30, no. 1 (2013): 272–280, https://doi.org/10.1016/j.foodhyd.2012.05.026.

65. J. Ebrahimi, M. G. Ahangari, and M. Jahanshahi, "Computational Studies at the Density Functional Theory (DFT) Level About the Surface Functionalization of Hexagonal Monolayers by Chitosan Monomer," *Applied Surface Science* 440 (2018): 778–789, https://doi.org/10.1016/j.apsusc.2018.01.210.

66. D. S. Bakirtzis, V. C. Tsapara, K. G. Kolovos, and S. E. Liodakis, "Assessment of the Impact of Fire Retardants on the Combustion of Natural Polymers Employing DTG and LOI," *Fire and Materials* 39, no. 2 (2015): 109–118, https://doi.org/10.1002/FAM.2232.

67. N. Hammi, M. Kędzierska, N. Wrońska, et al., "Boron Nitride Embedded in Chitosan Hydrogel as a Hydrophobic, Promising Metal-Free, Sustainable Antibacterial Material," *Materials Advances* 4, no. 21 (2023): 5191–5199, https://doi.org/10.1039/d3ma00445g.

68. F. Han Lyn, C. P. Tan, R. M. Zawawi, and Z. A. Nur Hanani, "Physicochemical Properties of Chitosan/ Graphene Oxide Composite Films and Their Effects on Storage Stability of Palm-Oil Based Margarine," *Food Hydrocolloids* 117 (2021): 106707, https://doi.org/10.1016/j.foodhyd.2021.106707.

69. K. Wang, X. Sun, F. Li, and D. Xie, "Enhanced Water Vapor Barrier and Gas Barrier Properties of Transparent Poly(Butylene Adipate-Co-Terephthalate)/poly(Lactic Acid)/hexagonal Boron Nitride Nanosheets Composite Films," *Materials Letters* 352 (2023): 135171, https://doi.org/10.1016/j.matlet.2023.135171.

70. Y. Liu, Y. Yuan, S. Duan, et al., "Preparation and Characterization of Chitosan Films With Three Kinds of Molecular Weight for Food Packaging," *International Journal of Biological Macromolecules* 155 (2020): 249–259, https://doi.org/10.1016/j.ijbiomac.2020.03.217.

71. A. R. Kamble, C. M. Patel, and Z. V. P. Murthy, "Effects of Inorganic Additive of Two-Dimensional Hexagonal Boron Nitride on the Gas Separation/Permeation for PVDF-Derived Membranes," *Separation Science and Technology* 54, no. 9 (2019): 1489–1501, https://doi.org/10.1080/01496395.2019.1577451.

72. I. Leceta, P. Guerrero, and v. K. De La Caba, "Functional Properties of Chitosan-Based Films," *Carbohydrate Polymers* 93 (2013): 339–346, https://doi.org/10.1016/j.carbpol.2012.04.031.

73. U. Jančič, M. Roschger, V. Hacker, B. Genorio, D. Fakin, and S. Gorgieva, "High Oxygen Barrier Chitosan Films Neutralized by Alkaline Nanoparticles," *Cellulose* 28, no. 16 (2021): 10457–10475, https://doi.org/10.1007/s10570-021-04195-w.

74. E. A. Takara, J. Marchese, and N. A. Ochoa, "NaOH Treatment of Chitosan Films: Impact on Macromolecular Structure and Film Properties," *Carbohydrate Polymers* c. 132 (2015): 25–30, https://doi.org/10.1016/j.carbpol.2015.05.077.

75. P. P. Zuo, H.-F. Feng, Z.-Z. Xu, et al., "Fabrication of Biocompatible and Mechanically Reinforced Graphene Oxide-Chitosan Nanocomposite Films," *Chemistry Central Journal* 7, no. 1 (2013): 1–11, https://doi.org/10.1186/1752-153X-7-39.

76. D. L. Zimmerman and R. W. Jones, "Sem Analysis of Polymeric Mechanical Failures in Polyetherimide," *International Journal of Polymeric Materials and Polymeric Biomaterials* 23, no. 3–4 (1994): 151–165, https://doi.org/10.1080/00914039408029327.

77. J. D. G. R. William and D. Callister, *Materials Science and Engineering* 42, (Elsevier, 1980), 524–540.

78. M. Oh, W. Dong, K. Mao, Z. Taehyeong, and K. Dayoung, "Mechanical Behavior of ABS Plastic - Matrix Nanocomposites With Three Different Carbon - Based Nanofillers," *Polymer Bulletin* 78, no. 7 (2021): 3751–3762, https://doi.org/10.1007/s00289-020-03299-w.